Strong control of spin torque nano-oscillator linewidth using He + irradiation

Sheng Jiang, Roman Khymyn, Sunjae Chung, Tuan Quang Le, Liza Herrera Diez, Afshin Houshang, Mohammad Zahedinejad, Dafiné Ravelosona, Johan Åkerman

FULL ARTICLE

Strong control of spin torque nano-oscillator linewidth using He^+ irradiation

Sheng Jiang PhD[1,2*] | Roman Khymyn PhD[2] | Sunjae Chung PhD[2,3] | Quang Tuan Le PhD[1] | Liza Herrera Diez PhD[4] | Afshin Houshang PhD[2] | Mohammad Zahedinejad PhD[2] | Dafiné Ravelosona Professor[4,5] | Johan Åkerman Professor[1,2,6]

[1]Department of Applied Physics, School of Engineering Sciences, KTH Royal Institute of Technology, Electrum 229, 164 40 Kista, Sweden

[2]Physics Department, University of Gothenburg, 412 96, Gothenburg, Sweden

[3]Department of Physics Education, Korea National University of Education, Cheongju 28173, Korea

[4]Institut d'Electronique Fondamentale, CNRS, Université Paris-Sud, Université Paris-Saclay, 91405 Orsay, France

[5]Spin-Ion Technologies, 28 rue du Général Leclerc, 78000 Versailles Cedex, France

[6]NanOsc AB, 164 40 Kista, Sweden

Correspondence
Sheng Jiang PhD, Department of Applied Physics, School of Engineering Sciences, KTH Royal Institute of Technology, Electrum 229, 164 40 Kista, Sweden
Email: shengji@kth.se

Funding information

We demonstrate a new approach for improving the spectral linewidth of a spin torque nano-oscillator (STNO). Using He^+ ion irradiation, we tune the perpendicular magnetic anisotropy (PMA) of the STNO free layer such that its easy axis is gradually varied from strongly out-of-plane to moderate in-plane. As the PMA impacts the non-linearity $\mathcal{N}$ of the STNO, we can in this way control the threshold current, the current tunability of the frequency, and, in particular, the STNO linewidth, which dramatically improves by two orders of magnitude. Our results are in good agreement with the theory for nonlinear auto-oscillators, confirm theoretical predictions of the role of the nonlinearity, and demonstrate a straightforward path towards improving the microwave properties of STNOs.

KEYWORDS
spin-torque nano-oscillators, He^+ irradiation, perpendicular magnetic anisotropy

1 | INTRODUCTION

Spin-torque nano-oscillators (STNOs) are among the most promising candidates for nanoscale broadband microwave generators[1, 2, 3, 4, 5, 6] and detectors.[7, 8, 9] STNOs can generate broadband microwave frequencies ranging from hundreds of MHz to the sub-THz,[10, 11, 12, 13] controlled by both magnetic fields and dc currents.[5, 14] Moreover, the device size can be reduced to a few tens of nanometers, which is of great opportunity for industrial applications. They can also host a range of novel magnetodynamical spin wave modes, such as propagating spin waves of different orders,[15, 16] and magnetodynamical solitons, such as spin wave bullets[15] and droplets.[3]

However, the applicability of these devices has suffered from their low power emission and large linewidth. Nonlinear auto-oscillator theory[17, 18, 19, 20] explains the large linewidth as a consequence of the strong nonlinearity $\mathcal{N}$, *i.e.* the dependence of the microwave frequency on its precession amplitude. $\mathcal{N}$ can be controlled not only by the magnitude and direction of the magnetic field,[14, 21, 22, 23, 24, 25] but also by the magnetic properties of the free layer of the STNO, such as the magnetic anisotropy and the effective magnetization.[20] For instance, in an easy-plane free layer, $\mathcal{N}$ changes gradually from positive to negative values as the direction of magnetic field rotates from out-of-plane to in-plane.[17, 20] Several experimental studies have corroborated [14, 15, 17, 22, 26, 27, 28] this theoretical prediction, as the linewidth can be minimized when $\mathcal{N}$ approaches to zero at the critical angle of magnetic field. This can show a way how to improve the linewidth by selectively reducing $\mathcal{N}$.

Whereas all previous studies, which aimed at minimizing the $\mathcal{N}$, have focused only on varying the direction and magnitude of magnetic field on single device, and this minimal $\mathcal{N}$ can be achieved at a narrow range of conditions, limited generating frequency, and which will require a complicate design for applications as microwave generators. In our work, we therefore study systematically how $\mathcal{N}$ is affected by the strength of perpendicular magnetic anisotropy (PMA) H_k in a set of nanocontact (NC) STNOs with a [Co/Pd]/Cu/[Co/Ni] spin valve structure. To engineer the PMA, we utilize He^+ irradiation to modify the interface/surface of [Co/Ni] multilayer where the PMA is originated from and sensitive to.[29, 30, 31, 32] We show how $\mathcal{N}$ can be continuously tuned as H_k is controlled by He^+ irradiation fluence in otherwise identical devices. Most importantly, the linewidth is dramatically improved at moderate H_k values, where $\mathcal{N} \rightarrow 0$. Finally, we show excellent agreement of our experimental results with nonlinear auto-oscillator theory.[20]

2 | RESULTS AND DISCUSSION

It is well known that irradiation with Ar^+, He^+, and/or Ga^+ can be utilized to tune the magnetic properties of thin films by modifying the microstructure of the magnetic material.[29, 33] Here, we use He^+ irradiation to engineer the PMA of the [Co/Ni] multilayer free layer in all-perpendicular STNOs, since the PMA of magnetic multilayers is highly sensitive to its surface or interface characteristic.[31, 34, 35] He^+ irradiation was hence implemented as a separate step in our device fabrication recipe (see details in the **Experimental Section**). The devices were irradiated with the fluence F varied from 6 to 20×10^{14} He^+/cm^2.[36] Figure 1a shows a schematic of the irradiation process during the device fabrication. First, the magnetoresistance (MR) was measured in a perpendicular magnetic field (see the inset of Figure 1b). The MR is slightly degraded but remains better than 1% even for the highest fluence (Figure 1b). This confirms that the SV structure remains of a good quality. Second, spin-torque ferromagnetic resonance (ST-FMR)[37, 38, 39, 40, 41] measurements were performed to determine the effective magnetization, $\mu_0 M_{eff} = \mu_0 M_s - \mu_0 H_k$ [H_k being the perpendicular magnetic anisotropy (PMA)] of [Co/Ni] free layers. Figure 1c inset shows a representative spectrum of ST-FMR at $f = 34$ GHz at $F = 6\times10^{14}$ He^+/cm^2.[36] The signals exhibit one main peak and one side peak. The main peak is identified as the ferromagnetic resonance (FMR) peak, and the additional side peak

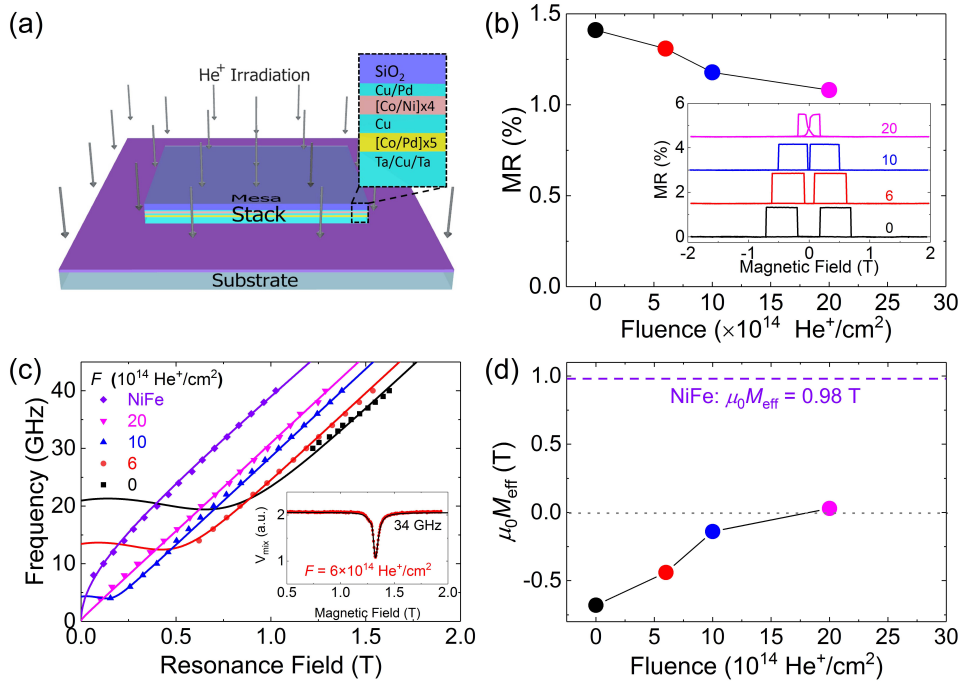

FIGURE 1 (a) A schematic of He^+ irradiation process and stack information. (b) Magnetoresistance (MR) as a function of irradiation fluence, obtained by sweeping perpendicular fields in the inset, where the numbers indicate the fluence F with a unit of 10^{14} He^+/cm^2. (c) Extracted main resonant fields at various frequencies: the solid lines are fits using the Kittel equation [Equation (1) and (2)]. The inset shows a representative ST-FMR spectrum at $f = 34$ GHz for $F = 6 \times 10^{14}$ He^+/cm^2. (d) The obtained effective magnetization $\mu_0 M_{\text{eff}}$ versus the irradiation fluence, and the dashed line shows the value of the NiFe free layer.

at lower field may result from spin-wave resonances, as studied in detail in Ref. MasoumehPRB2016. We then fit the spectra using two peaks with both symmetric and antisymmetric contributions as shown by the red line in the inset of Figure 1c. The main FMR fields at different frequencies are utilized and presented in Figure 1c. The FMR field is fitted by the universal Kittel equation[42, 23]

$$f = \frac{\gamma \mu_0}{2\pi} \sqrt{H_{\text{int}} \left(H_{\text{int}} + M_{\text{eff}} \cdot \cos^2 \theta_{\text{int}} \right)}, \tag{1}$$

where H_{int} and θ_{int} are the internal field and angle; their values are determined by solving for the magnetostatic equilibrium conditions:

$$\begin{aligned} H \cdot \cos \theta_{\text{ext}} &= H_{\text{int}} \cdot \cos \theta_{\text{int}} \\ H \cdot \sin \theta_{\text{ext}} &= (H_{\text{int}} + M_{\text{eff}}) \cdot \sin \theta_{\text{int}}, \end{aligned} \tag{2}$$

where $\theta_{\text{ext}} = 10^\circ$ is the applied field angle. The saturation magnetization $\mu_0 M_s = 1.1$ T of [Co/Ni] was found to be independent of He^+ irradiation, as previously measured by alternating gradient magnetometry.[36] Note that here NiFe (Permalloy) free layer has been used as a reference of in-plane magnetic anisotropy (IMA) with stronger M_{eff}. By

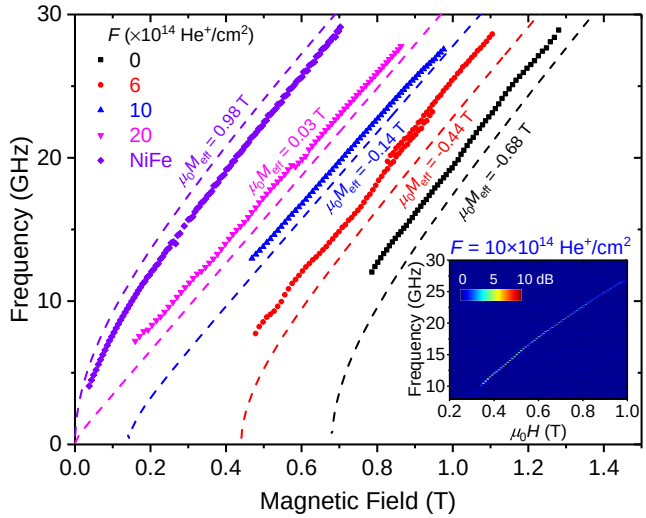

FIGURE 2 Auto-oscillation frequency versus in-plane magnetic field for various irradiated STNOs with R_{NC} = 35 nm. The dashed lines are the calculated FMR frequencies f_{FMR}, based on the values of $\mu_0 M_{eff}$ obtained from ST-FMR measurements. Inset: A typical power spectral density (PSD) of an STNO with F = 10×10^{14} He$^+$/cm^2 at I_{dc} = −14 mA.

fitting frequency vs. the resonance field with Equation (1) and (2), which are shown as solid lines in Figure 1c, the values of $\mu_0 M_{eff}$ for all samples are obtained and summarized in Figure 1d.

In Figure 2, we compare the calculated FMR frequency, f_{FMR}, using the measured M_{eff}, with the microwave signals generated from the STNO devices. The inset in Figure 2 shows a typical power spectral density (PSD) of the microwave signals for a fluence of $F = 10 \times 10^{14}$ He$^+$/cm^2. All PSD spectra are well fitted with a Lorentz function, and the extracted frequency f versus magnetic field is presented in Figure 2 with different symbols for each different fluence. All data show a quasi-linear dependence on the magnetic field, and the generated microwave frequency f extends to lower values as M_{eff} (H_k) increases (decreases). This behavior is consistent with the calculated value of the FMR frequency f_{FMR}, plotted as dashed lines in Figure 2. The overall trends of f_{FMR} are in good agreement with the auto-oscillation f. The difference between the calculated f_{FMR} and the measured auto-oscillation f is a direct measure of the nonlinearity of the magnetization precession,[43, 24, 15, 5] which is discussed in detail below. We note that there are double peaks at around 0.9 T fields for $F = 6 \times 10^{14}$ He$^+$/cm^2. This double peak phenomenon is infrequent and happens randomly between devices. It is likely an apparent effect of mode hopping between two closely spaced auto-oscillation modes. The sputtered [Co/Ni] films are polycrystalline and it is possible that grain boundaries underneath the nano-contact can impact the auto-oscillation modes from device to device and lead to slightly different local modes.

We now turn to the current-induced frequency tunability. Figure 3a–e shows the generated microwave frequency f versus dc current I_{dc} at a fixed magnetic field, $\mu_0 H$ = 0.72 T; f linearly depends on the I_{dc} at different values of M_{eff}. The current-induced frequency tunability df/dI_{dc} can be extracted from the slopes of linear fits which plot as each dashed line in Figure 3a–e. df/dI_{dc} for M_{eff} are then summarized in Figure 3f. We found that *i*) df/dI_{dc} decreases from 0.50 GHz/mA for nonirradiated [Co/Ni] to -0.13 GHz/mA for NiFe as M_{eff} increases (or H_k decreases), *ii*) the sign of df/dI_{dc} changes from positive (for [Co/Ni]) to negative (for NiFe), consistent with the easy axis transition from

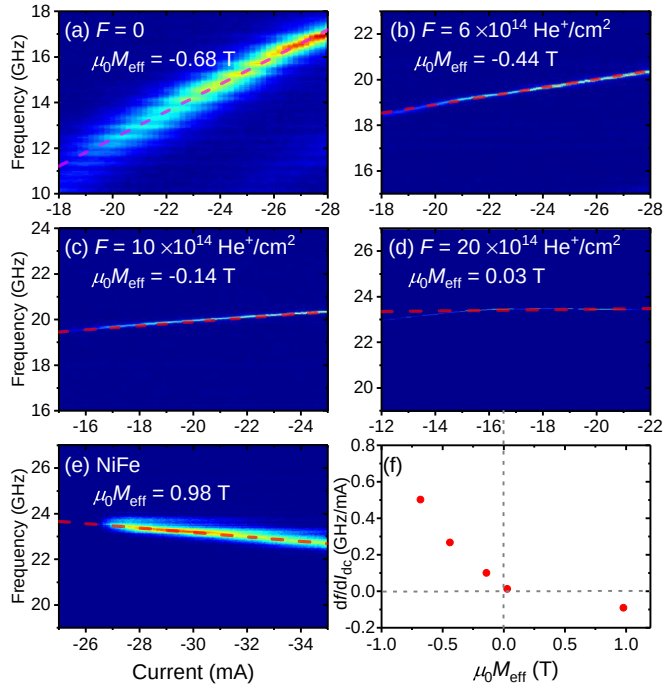

FIGURE 3 (a)–(e) PSD versus I_{dc} in STNOs with different irradiated fluences at $\mu_0 H = 0.72$ T. The red dotted line represents the linear fits of the auto-oscillation frequency. (f) slope df/dI_{dc} versus $\mu_0 M_{eff}$ extracted from the fits of (a)–(e).

out-of-plane for [Co/Ni] to in-plane for NiFe, and further details will be discussed later.

We carried out detailed measurements at different magnetic fields to understand further the behavior of df/dI_{dc}. Figure 4a shows one example of extracted f versus I_{dc} at different fields, ranging from 0.37 to 1.12 T with a 0.05 T step, for $F = 6\times10^{14}$ He$^+$/cm^2. All data show clear linear dependencies on I_{dc}. Here we would like to define one numerical relation about the tunability, $df/d\zeta = I_{th}(df/dI_{dc})$, to compare our experimental results directly with theoretical calculation, where $\zeta = I_{dc}/I_{th}$ is the dimensionless supercriticality parameter[20] and I_{th} is the threshold current. I_{th} were extracted from plots of inverse power $1/P$ versus I_{dc} as described in the **Supplemental Materials**. After obtained all I_{th} and df/dI_{dc} for different M_{eff}, $df/d\zeta$ are represented as solid dots in Figure 4b. All $df/d\zeta$ for different M_{eff} show similar behaviors that is inverse proportional to magnetic field. It is noteworthy that the overall $df/d\zeta$ decreases as M_{eff} (H_k) increases (decreases). It reaches around zero when the $\mu_0 M_{eff} \approx 0$ for $F = 20\times10^{14}$ He$^+$/cm^2. The sign of $df/d\zeta$ for NiFe is even negative.

To understand the behavior of tunability versus M_{eff} (H_k) from He$^+$-irradiated STNOs, we considered the nonlinear auto-oscillator theory of A. Slavin and V. Tiberkevich,[44, 43, 19, 20] which was derived from universal auto-oscillation systems and has proved to be consistent with the Landau–Lifshitz–Gilbert–Slonczewski (LLGS) equation.[20] This theory allows us to describe the experimental observation analytically. The auto-oscillation frequency f generated from an STNO is expressed as:

$$f(I_{dc}) = f_{FMR} + \frac{\mathcal{N}}{2\pi}\frac{\zeta - 1}{\zeta + Q}, \tag{3}$$

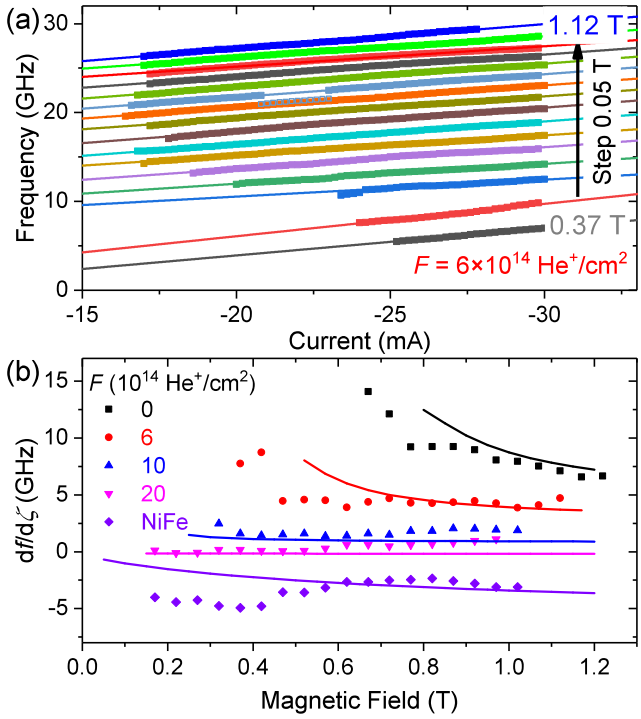

FIGURE 4 (a) Extracted auto-oscillation frequency f vs. I_{dc} at different magnetic fields for $F = 6\times10^{14}$ He^+/cm^2. Some minor frequency jumps at $\mu_0 H = 0.87$ T are shown as rectangular boxes, possibly due to film inhomogeneities generating different dynamical behaviors. (b) $df/d\zeta$ [*i.e.* $I_{th}(df/dI_{dc})$] vs. magnetic field, where I_{th} is extracted from the intercept of the inverse power of the auto-oscillation signals and the df/dI_{dc} are the slopes of the linear fits of frequency as $I_{dc} > I_{th}$ (see the Appendix). The solid lines are the theoretical calculation from Equation (4)–(6).

where $\mathcal{N}$ is the nonlinearity factor, $\frac{\zeta-1}{\zeta+Q} = P$ is the normalized power of the stationary precession, and Q is the nonlinear damping coefficient. From Equation (3), the frequency shift is mainly decided by the nonlinearity $\mathcal{N}$. Taking the derivation of Equation (3), $df/d\zeta$ is derived as:

$$\frac{df}{d\zeta} = I_{th}\frac{df}{dI_{dc}} = \frac{\mathcal{N}}{2\pi}\frac{1+Q}{(\zeta+Q)^2}. \tag{4}$$

The nonlinear frequency shift coefficient $\mathcal{N}$ for STNOs dominates the frequency tunability, and may be positive, zero, or negative, depending on magnetic field direction and magnetic anisotropy of free layer in STNOs.

To explain the experimental observations using this analytical theory, we derive $\mathcal{N}$ with our experimental conditions. The nonlinearity is expressed as[43]

$$\mathcal{N} = -\frac{\omega_H\omega_M(\omega_H+\omega_M/4)}{\omega_0(\omega_H+\omega_M/2)}, \tag{5}$$

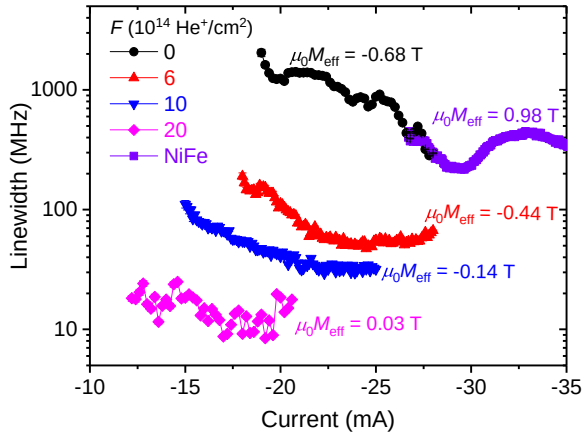

FIGURE 5 Linewidth Δf versus I_{dc} with different effective magnetization $\mu_0 M_{eff}$ at $\mu_0 H = 0.72$ T. The linewidth were extracted from the data in Figure 3a–e.

$$\begin{cases} \omega_H = \gamma H \\ \omega_M = 4\pi\gamma M_{eff} \\ \omega_0 = \gamma\sqrt{\omega_H\,(\omega_H + \omega_M)}. \end{cases} \tag{6}$$

We note that Equation (5) and (6) are valid for the magnetization of the free layer being aligned to the magnetic field direction. Utilizing Equation (5) and (6), we calculate $df/d\zeta$ ($\propto \mathcal{N}$), where ζ and Q are used as fitting parameters for all data in Figure 4b, and we find reasonable good agreements with 1.5 for ζ and 3.0 for Q, respectively. All calculated results are shown as the solid lines alongside the experimental results in Figure 4b. It should be noted that the theoretical calculation coincides with experimental results in the overall trend, although there are discrepancies between experiment and theory. One reason for these discrepancies is likely that the theory does not take into account the current-induced Joule heating and Oersted fields that are present in the experiments. In addition, the calculated nonlinearity $\mathcal{N}$ can also explain the frequency difference between the calculated f_{FMR} and the generated microwave frequency f in Figure 1. Due to the negative value of $\mathcal{N}$ (or $df/d\zeta$) for NiFe, f is expected to be lower than f_{FMR}, as predicted in Equation (3) and consistent with our experimental observations in Figure 2. This auto-oscillation mode is often characterized as a localized bullet.[14, 15, 43] In contrast, $\mathcal{N}$ is positive for easy out-of-plane [Co/Ni], so $f > f_{FMR}$ in Figure 2.[14, 43, 45] In this case, its mode favors to be a propagating spin-wave.[14, 28, 46] All of these experimental observations confirm the theoretical predictions very well.

Furthermore, according to nonlinear auto-oscillator theory, the linewidth Δf of the generated microwave signals can be expressed as[20]

$$\Delta f = \Gamma_+ \frac{k_B T}{E(P)}\left[1 + \left(\frac{\mathcal{N}}{\Gamma_{eff}}\right)^2\right], \tag{7}$$

where k_B is the Boltzmann constant and T is the temperature. Γ_+ and $E(P)$ are the damping function and time-averaged oscillation energy as a function of the power P, respectively. Γ_{eff} is the effective damping. In Equation(7), the linewidth Δf exhibits a quadratic dependence on the nonlinearity $\mathcal{N}$. To compare with our experimental results, we extracted the linewidth from the data in Figure 3a–e, as shown in Figure 5. The linewidth was indeed dramatically

improved by about two orders of magnitude as $\mathcal{N}$ decreases (as M_{eff} increases), it reaches to a lowest value for $\mu_0 M_{\text{eff}} = 0.03$ T, where $\mathcal{N} \to 0$. Δf again increases for the NiFe free layer when $\mathcal{N}$ becomes moderately negative. There are also contributions due to the variation of other parameters, like Γ_+, Γ_{eff}, and $E(P)$. The values Γ_+ and Γ_{eff} are proportional to the damping constant α,[47] however, it only changes by about a factor of 2 at $F = 20\times10^{14}$ He^+/cm^2 as compare to the non-irradiated one.[36] The oscillation energy $E(P)$ for the circular precession can be assumed as $E(P) \propto \sin\theta$,[20, 47] where θ is the precessional angle, which can be derived from the experimental output power $P_{\text{out}} \sim \text{GMR} \sin\theta \sin\beta$.[26] Here β is the relative angle of the magnetization between the free and fixed layer. GMR is the ratio of giant magnetoresistance. We found that $E(P)$, calculated from the values in Ref. Jiang2018a, only shows $\sim 10\%$ reduction by He^+ irradiation. In fact, we are able to fit the experimental data shown in Figure 4b with a single value of the nonlinear damping Q and supercriticality ζ for the all irradiation fluences. That particularly means that the power $P = (\zeta - 1)/(\zeta + Q)$ also remains the same, so does $E(P)$. We therefore argue that decreasing of $\mathcal{N}$ dominates the linewidth reduction, while the variation of other parameters in Equation (7) has a minor contribution.

The excellent agreement between our experimental results and theory confirms that the linewidth can be minimized intentionally by controlling the nonlinearity in general, and tuning it to zero in particular. When the PMA compensates the demagnetization field, the nonlinearity identically equals zero regardless of the external conditions. We can therefore minimize the linewidth by choosing free layer materials with $\mu_0 M_{\text{eff}} \to 0$. We hence would emphasize that our study can offers a universal path to solving one of the key issues in utilizing STNOs as microwave generators. As for the generated microwave power—another key drawback of this type of microwave generators—we did not observe an improvement in this study, mainly due to the slightly degradation in MR values.[36] We expect that the power can be dramatically improved using magnetic tunnel junction-based STNOs, whose MR can be over two orders of magnitude greater than that of spin valve-based STNOs.[2, 16]

3 | CONCLUSION

In conclusion, we have presented a systematic study of the variation of nonlinearity against PMA in STNOs. By using He^+ irradiation to continuously tune the PMA of the [Co/Ni] free layer, the nonlinearity $\mathcal{N}$ (along with the frequency tunability df/dI_{dc}) shows a continuous decreasing trend as H_{k} (M_{eff}) decreases (increases). As a consequence of this decreasing nonlinearity, we have achieved an approximately hundredfold improvement in the linewidth. Our experimental observations are in excellent agreement with nonlinear auto-oscillator theory. This systematic study not only verifies the theoretical prediction, but also offers a route to improving the linewidth—selecting a free layer's material whose $M_{\text{eff}} \to 0$, which is of great importance for commercializing microwave generators.

4 | EXPERIMENTAL SECTION

Device Fabrication and He^+ Irradiation The STNO devices were fabricated from all-perpendicular (all-PMA) [Co/Pd/Cu/[Co/Ni][36, 45] and orthogonal [Co/Pd]/Cu/NiFe spin valves (SVs). The full stack consists of a Ta (5)/Cu (15)/Ta (5)/Pd (3) seed layer, an all-PMA [Co (0.5)/Pd (1.0)]×5/Cu (7)/[Co (0.3)/Ni (0.9)]×4/Co (0.3) or orthogonal [Co (0.5)/Pd (1.0)]×5/Cu (7)/$Ni_{80}Fe_{20}$ (4.5) SV with a Cu(3)/Pd(3) capping layer (here NiFe is served as a reference with ignorable PMA), sputtered onto a thermally oxidized 100 mm Si wafer (numbers in parentheses are layer thicknesses in nanometers). The deposited stacks were first patterned into 8 μm × 20 μm mesas using photolithography and ion-milling etching, followed by chemical vapor deposition (CVD) of an insulating 40-nm-thick SiO_2 film. Electron beam lithography and reactive ion etching were used to open nanocontacts (with nominal radius of R_{NC} 35 nm) through the SiO_2 in the

center of each mesa. The processed wafer was then cut into different pieces for He^+ irradiation with the fluence F varied from 6 to 20×10^{14} He^+/cm^2.[36] This is done by a commercial irradiation facility with highly uniform ion beam in millimeter-scale. Fabrication was completed with lift-off lithography and deposition of a Cu (500 nm)/Au (100 nm) top electrode in a single run with all irradiated pieces. Our protocol hence ensures that all other properties, except the He^+ fluence, are identical from device to device.

Spin-torque Ferromagnetic Resonance ST-FMR involves using a microwave generator (capable of up to 40 GHz) to inject a fixed frequency through a bias-tee to a STNO, which is connected with a commercial picoprobe. The rf power is set to -2 dBm to avoid nonlinear magnetodynamics. The rf signal is modulated at a frequency of 313 Hz for lock-in detection.[39] The resulted mixing dc voltage[48] is measured by a lock-in amplifier. The magnetic field is swept from 0 to 2 T at a small (10°) out of plane angle as this produced cleaner resonances than in in-plane fields.

D.C. and Microwave characterization We used our custom-built probe station for static and microwave characterization. A direct current I_{dc} was injected into the devices using a Keithley 6221 current source, and the dc voltage was detected using a Keithley 2182 nanovoltmeter. The magnetic field was applied in the plane of the film. The generated microwave signals from the STNO device were decoupled from the dc voltage via a bias-tee, amplified using a low-noise amplifier, and then recorded with a spectrum analyzer.[49, 50]

Acknowledgements

This work was supported by the China Scholarship Council (CSC), the Swedish Foundation for Strategic Research (SSF), the Swedish Research Council (VR), and the Knut and Alice Wallenberg Foundation (KAW). Additional support for the work was provided by the European Research Council (ERC) under the European Community's Seventh Framework Programme (FP/2007-2013) /ERC Grant 307144 "MUSTANG".

Conflict of interest

The authors declare that they have no competing interests.

references

[1] A. M. Deac, A. Fukushima, H. Kubota, H. Maehara, Y. Suzuki, S. Yuasa, Y. Nagamine, K. Tsunekawa, D. D. Djayaprawira, N. Watanabe. *Nat. Phys.* **2008**, *4*, 10 803.

[2] H. Maehara, H. Kubota, Y. Suzuki, T. Seki, K. Nishimura, Y. Nagamine, K. Tsunekawa, A. Fukushima, A. M. Deac, K. Ando, S. Yuasa. *Appl. Phys. Express* **2013**, *6*, 11 113005.

[3] S. M. Mohseni, S. R. Sani, J. Persson, T. N. A. Nguyen, S. Chung, Y. Pogoryelov, P. K. Muduli, E. Iacocca, A. Eklund, R. K. Dumas, S. Bonetti, A. Deac, M. A. Hoefer, J. Åkerman. *Science* **2013**, *339*, 6125 1295.

[4] H. Maehara, H. Kubota, Y. Suzuki, T. Seki, K. Nishimura, Y. Nagamine, K. Tsunekawa, A. Fukushima, H. Arai, T. Taniguchi, H. Imamura, K. Ando, S. Yuasa. *Appl. Phys. Express* **2014**, *7*, 2 023003.

[5] T. Chen, R. K. Dumas, A. Eklund, P. K. Muduli, A. Houshang, A. A. Awad, P. Durrenfeld, B. G. Malm, A. Rusu, J. Åkerman. *Proc. IEEE* **2016**, *104*, 10 1919.

[6] S. A. H. Banuazizi, S. R. Sani, A. Eklund, M. M. Naiini, S. M. Mohseni, S. Chung, P. Dürrenfeld, B. G. Malm, J. Åkerman. *Nanoscale* **2017**, *9* 1896.

[7] P. M. Braganca, B. A. Gurney, B. A. Wilson, J. A. Katine, S. Maat, J. R. Childress. *Nanotechnology* **2010**, *21*, 23 235202.

[8] S. Miwa, S. Ishibashi, H. Tomita, T. Nozaki, E. Tamura, K. Ando, N. Mizuochi, T. Saruya, H. Kubota, K. Yakushiji, T. Taniguchi, H. Imamura, A. Fukushima, S. Yuasa, Y. Suzuki. *Nat. Mater.* **2014**, *13*, 1 50.

[9] B. Fang, M. Carpentieri, X. Hao, H. Jiang, J. A. Katine, I. N. Krivorotov, B. Ocker, J. Langer, K. L. Wang, B. Zhang, B. Azzerboni, P. K. Amiri, G. Finocchio, Z. Zeng. *Nat. Commun.* **2016**, *7* 11259.

[10] V. S. Pribiag, I. N. Krivorotov, G. D. Fuchs, P. M. Braganca, O. Ozatay, J. C. Sankey, D. C. Ralph, R. A. Buhrman. *Nat. Phys.* **2007**, *3*, 7 498.

[11] M. A. Hoefer, M. J. Ablowitz, B. Ilan, M. R. Pufall, T. J. Silva. *Phys. Rev. Lett.* **2005**, *95*, 26 267206.

[12] R. L. Stamps, S. Breitkreutz, J. Åkerman, A. V. Chumak, Y. Otani, G. E. W. Bauer, J.-U. Thiele, M. Bowen, S. A. Majetich, M. Kläui, I. L. Prejbeanu, B. Dieny, N. M. Dempsey, B. Hillebrands. *J. Phys. D. Appl. Phys.* **2014**, *47*, 33 333001.

[13] I. Lisenkov, R. Khymyn, J. Åkerman, N. X. Sun, B. A. Ivanov. *Phys. Rev. B* **2019**, *100* 100409.

[14] R. K. Dumas, E. Iacocca, S. Bonetti, S. R. Sani, S. M. Mohseni, A. Eklund, J. Persson, O. Heinonen, J. Åkerman. *Phys. Rev. Lett.* **2013**, *110*, 25 257202.

[15] S. Bonetti, V. Tiberkevich, G. Consolo, G. Finocchio, P. Muduli, F. Mancoff, A. Slavin, J. Åkerman. *Phys. Rev. Lett.* **2010**, *105*, 21 217204.

[16] A. Houshang, R. Khymyn, M. Dvornik, M. Haidar, S. R. Etesami, R. Ferreira, P. P. Freitas, R. K. Dumas, J. Åkerman. *Nat. Commun.* **2018**, *9*, 2018 4374.

[17] J. V. Kim, V. Tiberkevich, A. N. Slavin. *Phys. Rev. Lett.* **2008**, *100*, 1 017207.

[18] J. V. Kim, Q. Mistral, C. Chappert, V. S. Tiberkevich, A. N. Slavin. *Phys. Rev. Lett.* **2008**, *100*, 16 167201.

[19] A. Slavin, V. Tiberkevich. *IEEE Trans. Magn.* **2008**, *44*, 7 1916.

[20] A. Slavin, V. Tiberkevich. *IEEE Trans. Magn.* **2009**, *45*, 4 1875.

[21] M. R. Pufall, W. H. Rippard, S. E. Russek, S. Kaka, J. A. Katine. *Phys. Rev. Lett.* **2006**, *97*, 8 087206.

[22] W. H. Rippard, M. R. Pufall, S. E. Russek. *Phys. Rev. B* **2006**, *74*, 22 224409.

[23] G. Gerhart, E. Bankowski, G. A. Melkov, V. S. Tiberkevich, A. N. Slavin. *Phys. Rev. B* **2007**, *76* 024437.

[24] G. Consolo, B. Azzerboni, L. Lopez-Diaz, G. Gerhart, E. Bankowski, V. Tiberkevich, A. N. Slavin. *Phys. Rev. B* **2008**, *78*, 1 014420.

[25] P. K. Muduli, Y. Pogoryelov, S. Bonetti, G. Consolo, F. Mancoff, J. Åkerman. *Phys. Rev. B* **2010**, *81*, 14 140408(R).

[26] S. Bonetti, V. Puliafito, G. Consolo, V. S. Tiberkevich, A. N. Slavin, J. Åkerman. *Phy. Rev. B* **2012**, *85* 174427.

[27] O. J. Lee, P. M. Braganca, V. S. Pribiag, D. C. Ralph, R. A. Buhrman. *Phys. Rev. B* **2013**, *88*, 22 224411.

[28] M. Mohseni, M. Hamdi, H. F. Yazdi, S. A. H. Banuazizi, S. Chung, S. R. Sani, J. Åkerman, M. Mohseni. *Phys. Rev. B* **2018**, *97*, 18 184402.

[29] C. Chappert, H. Bernas, J. Ferre, V. Kottler, J.-P. Jamet, Y. Chen, E. Cambril, T. Devolder, F. Rousseaux, V. Mathet, H. Launois. *Science* **1998**, *280*, 5371 1919.

[30] J. Fassbender, D. Ravelosona, Y. Samson. *J. Phys. D: Appl. Phys.* **2004**, *37*, 16 R179.

[31] J.-M. Beaujour, D. Ravelosona, I. Tudosa, E. E. Fullerton, A. D. Kent. *Phys. Rev. B* **2009**, *80*, 18 180415(R).

[32] D. L. Herrera, F. García-Sánchez, J.-P. Adam, T. Devolder, S. Eimer, M. S. El Hadri, A. Lamperti, R. Mantovan, B. Ocker, D. Ravelosona. *Appl. Phys. Lett.* **2015**, *107*, 3 032401.

[33] C. T. Rettner, S. Anders, J. E. E. Baglin, T. Thomson, B. D. Terris. *Appl. Phy. Lett.* **2002**, *80*, 2 279.

[34] D. Stanescu, D. Ravelosona, V. Mathet, C. Chappert, Y. Samson, C. Beigń, N. Vernier, J. Ferŕ, J. Gierak, E. Bouhris, E. E. Fullerton. *J. Appl. Phys.* **2008**, *103*, 103 07B529.

[35] J.-M. L. Beaujour, A. D. Kent, D. Ravelosona, I. Tudosa, E. E. Fullerton. *J. Appl. Phys.* **2011**, *109*, 3 033917.

[36] S. Jiang, S. Chung, L. H. Diez, T. Q. Le, F. Magnusson, D. Ravelosona, J. Åkerman. *AIP Adv.* **2018**, *8* 065309.

[37] Y. Okutomi, K. Miyake, M. Doi, H. N. Fuke, H. Iwasaki, M. Sahashi. *J. Appl. Phys.* **2011**, *109*, 7 07C727.

[38] L. Liu, C. F. Pai, Y. Li, H. W. Tseng, D. C. Ralph, R. A. Buhrman. *Science* **2012**, *336* 555.

[39] M. Fazlali, M. Dvornik, E. Iacocca, P. Dürrenfeld, M. Haidar, J. Åkerman, R. K. Dumas. *Phys. Rev. B* **2016**, *93* 134427.

[40] H. Mazraati, S. Chung, A. Houshang, M. Dvornik, L. Piazza, F. Qejvanaj, S. Jiang, T. Q. Le, J. Weissenrieder, J. Åkerman. *Appl. Phys. Lett.* **2016**, *109*, 24 242402.

[41] M. Zahedinejad, H. Mazraati, H. Fulara, J. Yue, S. Jiang, A. A. Awad, J. Åkerman. *Appl. Phys. Lett.* **2018**, *112*, 13 132404.

[42] C. Kittel. *Phys. Rev.* **1949**, *76*, 6 743.

[43] A. Slavin, V. Tiberkevich. *Phys. Rev. Lett.* **2005**, *95*, 23 237201.

[44] A. N. Slavin, P. Kabos. *IEEE Trans. Magn.* **2005**, *41*, 4 1264.

[45] S. Chung, Q. T. Le, M. Ahlberg, A. A. Awad, M. Weigand, I. Bykova, R. Khymyn, M. Dvornik, H. Mazraati, A. Houshang, S. Jiang, T. N. A. Nguyen, E. Goering, G. Schütz, J. Gräfe, J. Åkerman. *Phys. Rev. Lett.* **2018**, *120*, 21 217204.

[46] M. Madami, E. Iacocca, S. Sani, G. Gubbiotti, S. Tacchi, R. K. Dumas, J. Åkerman, G. Carlotti. *Phys. Rev. B* **2015**, *92*, 2 024403.

[47] P. M. Braganca, B. A. Gurney, A. G. F. Garcia, J. A. Katine, J. R. Childress. *Phys. Rev. Appl.* **2015**, *4*, 1 014017.

[48] J. C. Sankey, P. M. Braganca, A. G. F. Garcia, I. N. Krivorotov, R. A. Buhrman, D. C. Ralph. *Phys. Rev. Lett.* **2006**, *96* 227601.

[49] S. Jiang, S. R. Etesami, S. Chung, Q. T. Le, A. Houshang, J. Åkerman. *IEEE Magn. Lett.* **2018**, *9* 3104304.

[50] S. Jiang, S. Chung, Q. T. Le, H. Mazraati, A. Houshang, J. Åkerman. *Phys. Rev. Appl.* **2018**, *10*, 5 054014.